Lipoxygenase mediates invasion of intrametastatic lymphatic vessels and propagates lymph node metastasis of human mammary carcinoma xenografts in mouse

Dontscho Kerjaschki,[1,2] Zsuzsanna Bago-Horvath,[1,2,3] Margaretha Rudas,[1,2,3] Veronika Sexl,[4] Christine Schneckenleithner,[4] Susanne Wolbank,[5] Gregor Bartel,[1] Sigurd Krieger,[1] Romana Kalt,[1] Brigitte Hantusch,[1,2] Thomas Keller,[1] Katalin Nagy-Bojarszky,[1] Nicole Huttary,[1] Ingrid Raab,[1] Karin Lackner,[1] Katharina Krautgasser,[1] Helga Schachner,[1] Klaus Kaserer,[1] Sandra Rezar,[1] Sybille Madlener,[1] Caroline Vonach,[1] Agnes Davidovits,[1] Hitonari Nosaka,[1] Monika Hämmerle,[1] Katharina Viola,[1] Helmut Dolznig,[1] Martin Schreiber,[6] Alexander Nader,[7] Wolfgang Mikulits,[2,8] Michael Gnant,[2,3,9] Satoshi Hirakawa,[10] Michael Detmar,[11] Kari Alitalo,[12] Sebastian Nijman,[13] Felix Offner,[14] Thorsten J. Maier,[15] Dieter Steinhilber,[15] and Georg Krupitza[1,2]

[1]Clinical Institute of Pathology, [2]Comprehensive Cancer Center, [3]Austrian Breast and Colorectal Cancer Study Group (ABCSG), and [4]Institute of Pharmacology, Medical University of Vienna, Vienna, Austria. [5]Ludwig Boltzmann Institute for Experimental and Clinical Traumatology, Vienna, Austria. [6]Department of Gynaecology, Medical University of Vienna, Vienna, Austria. [7]Pathology Institute, Hanusch Hospital, Vienna, Austria. [8]Institute of Cancer Research and [9]Department of Surgery, Medical University of Vienna, Vienna, Austria. [10]Department of Dermatology, Ehime University Graduate School of Medicine, Ehime, Japan. [11]Department of Pharmacogenomics, Swiss Federal Institute of Technology ETH-Zurich, Zurich, Switzerland. [12]Molecular/Cancer Biology Laboratory, Biomedicum Helsinki, University of Helsinki, Helsinki, Finland. [13]Ce-M-M-Research Center for Molecular Medicine of the Austrian Academy of Sciences, Vienna, Austria. [14]Institute for Pathology, LKH Feldkirch, Austria. [15]Institute of Pharmaceutical Chemistry/ZAFES, Frankfurt/Main, Germany.

In individuals with mammary carcinoma, the most relevant prognostic predictor of distant organ metastasis and clinical outcome is the status of axillary lymph node metastasis. Metastases form initially in axillary sentinel lymph nodes and progress via connecting lymphatic vessels into postsentinel lymph nodes. However, the mechanisms of consecutive lymph node colonization are unknown. Through the analysis of human mammary carcinomas and their matching axillary lymph nodes, we show here that intrametastatic lymphatic vessels and bulk tumor cell invasion into these vessels highly correlate with formation of postsentinel metastasis. In an in vitro model of tumor bulk invasion, human mammary carcinoma cells caused circular defects in lymphatic endothelial monolayers. These circular defects were highly reminiscent of defects of the lymphovascular walls at sites of tumor invasion in vivo and were primarily generated by the tumor-derived arachidonic acid metabolite 12S-HETE following 15-lipoxygenase-1 (ALOX15) catalysis. Accordingly, pharmacological inhibition and shRNA knockdown of ALOX15 each repressed formation of circular defects in vitro. Importantly, ALOX15 knockdown antagonized formation of lymph node metastasis in xenografted tumors. Furthermore, expression of lipoxygenase in human sentinel lymph node metastases correlated inversely with metastasis-free survival. These results provide evidence that lipoxygenase serves as a mediator of tumor cell invasion into lymphatic vessels and formation of lymph node metastasis in ductal mammary carcinomas.

Introduction

A tumor's metastatic potential is determined by complex and specific genetic gains and/or losses of function that enable tumor cells to emigrate from their primary site to access the blood or lymphatic vasculature and to form premetastatic niches in target organs that provide the essential "soil" for "seeding" of incoming tumor cells (1). Despite the obvious clinical relevance of these events, relatively little is currently known about the underlying mechanisms. For example, only some aspects of niche formation in distant organs have been identified; these include local accumulation of bone marrow–derived cells, fibronectin deposition (2), and interactions between tumor cells and thrombocytes (3).

Whether tumors metastasize initially into lymph nodes or are distributed by hematogenous dissemination into distant organs remains a matter for debate, and there is experimental evidence for each hypothesis (4–6). One view holds that metastatic tumor cells colonize distant organs via the blood stream either from lymph nodes ("metastasis from metastasis") (7) or by cross seeding from the primary tumor by recirculation (8). Alternatively, clonogenic tumor cells, presumably with stem cell–like characteristics, could disseminate simultaneously at an early time point from primary tumors into both the blood and lymphatic vasculature and then develop metastases asynchronously in both compartments (9). Although currently evidence is accumulating in favor of the latter hypothesis (5), it falls short of explaining why the number of regional lymph nodes affected by metastases most accurately predicts the general extent of metastatic spreading and overall clinical outcome, for

Conflict of interest: The authors have declared that no conflict of interest exists.
Citation for this article: *J Clin Invest.* 2011;121(5):2000–2012. doi:10.1172/JCI44751.

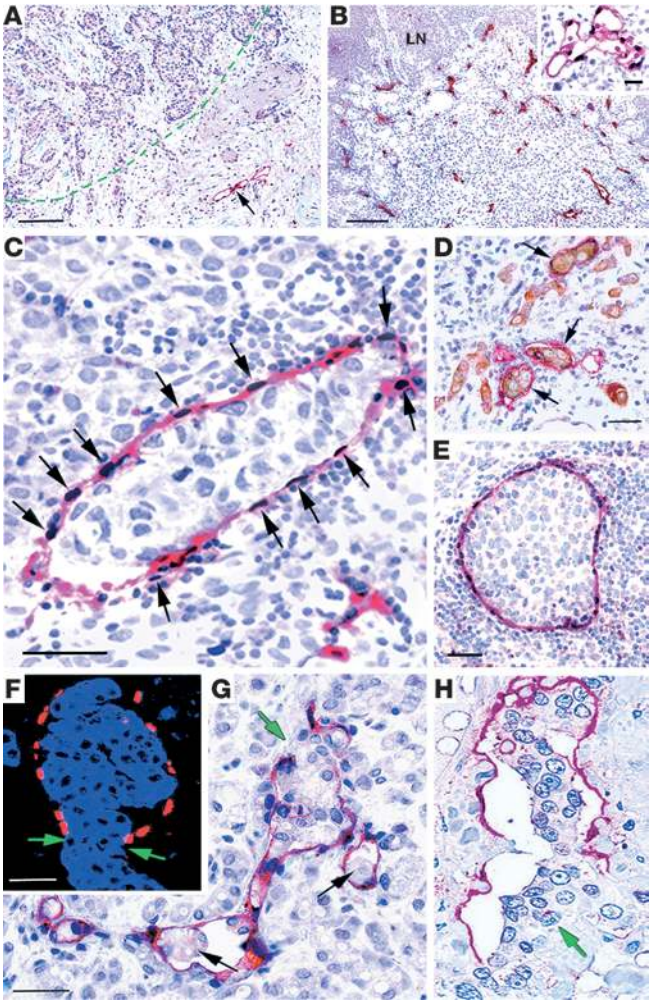

Figure 1
Intrametastatic lymphangiogenesis and tumor cell invasion into lymphatic vessels in sentinel lymph nodes of human ductal mammary carcinomas with postsentinel metastasis. Lymphatic endothelial cells are localized by double labeling for podoplanin (red) and PROX1 (black) in **A**–**C** and **E**. (**A**) In a primary ductal carcinoma, lymphatic vessels are localized in the peritumoral stroma (arrow). The tumor border is marked by a green line. (**B**) Sentinel lymph node metastasis of the same carcinoma as in part **A**, with dense intrametastatic lymphatic vascularization. LN, residual lymph node parenchyma. Insert, FLT4 (red) in an intrametastatic lymphatic vessel (PROX1, black). (**C**) High-power view of an intrametastatic lymphatic vessel with podoplanin$^+$ lymphatic endothelial cells and PROX1-expressing nuclei (arrows). The vessel contains a tumor embolus and is surrounded by mononuclear inflammatory or tumor cells. (**D**) Keratin$^+$ tumor cell emboli (brown) within intrametastatic lymphatic vessels with podoplanin$^+$ endothelial cells (red). (**E**) Large tumor embolus completely filling the lumen of an intrametastatic lymphatic vessel. (**F**) Aggregate of keratin$^+$ carcinoma cells disrupts an intrametastatic lymphatic vessel that is outlined by a single line of PROX1$^+$ nuclei (red). The margins of the vessel's rupture are indicated by green arrows. (**G** and **H**) Embolic tumor cell clusters (black arrows) within a branched intrametastatic lymphatic vessel, and a focal disruption of the lymphatic vascular wall by a bulk of aggregated tumor cells (green arrow). The lymphatic vessel's walls are composed of a single endothelial layer. Scale bars: 100 μm; 25 μm (insert).

example, in mammary carcinomas. This well-established fact is reflected in clinically validated and diagnostically indispensable consensus systems used in routine histopathological mammary tumor staging (10, 11). Testing these hypotheses, which are not mutually exclusive, depends on better understanding of the so-far elusive molecular mechanisms that determine the initial tumor cells' specific preference for invasion of blood or lymphatic vessels to reach their respective target organs.

Here we have systematically analyzed the lymphometastatic properties of human mammary carcinomas. These have distinct advantages for such studies, including the anatomically conserved lymphatic draining patterns of the human breast (12) and their repetitive pattern of metastatic spreading. Thus, most mammary carcinomas form their initial metastasis in up to 3 axillary lymph node or nodes that receive afferent lymph from the tumor and peritumoral tissue and are designated as "sentinel lymph nodes." Further metastatic progression occurs by successive colonization of the postsentinel lymph nodes in the axillary basin. Previous work has shown that lymphangiogenesis in sentinel lymph node metastases correlates with postsentinel tumor spreading (13). In this study, we have addressed the mechanisms underlying this process, using immunohistochemistry with selective lymphatic endothelial markers (podoplanin, LYVE1, and PROX1) (14–16), in vitro models, and xenograft tumors. The findings are compatible with a context-specific reaction of lymphatic endothelial cells with tumor-derived products of lipoxygenases that is critical for tumor cell entry into the lymphatic vessel and metastatic spreading from the sentinel to postsentinel lymph nodes. The results also shed light on the fact that different tumor types use different means to invade intrametastatic lymphatics.

Results

Intrametastatic lymphatic carcinosis. We localized lymphatic endothelial cells in 104 precisely matched primary ductal and lobular mammary carcinomas (stages pT1c, N0, or N1a, or pooled stages N2 and N3; ref. 11 and Supplemental Table 1; supplemental material available online with this article; doi:10.1172/JCI44751DS1) and in their corresponding sentinel and postsentinel axillary lymph nodes (Figure 1). Lymphatic vessels were restricted to the peritumoral stroma (17) in all the primary carcinomas. In contrast, the sentinel lymph node metastases of these tumors were often endowed with lymphatic vessels connected to those in the residual sentinel lymph node's parenchyma (Supplemental Figure 1). Their endothelial cells expressed the major lymphatic markers FLT4 (VEGFR3), podoplanin, PROX1, and, with some variability, also LYVE1, as reported (18). The density of intrametastatic lymphatics and their endothelial mitotic rate were more than 2-fold higher than those in residual lymph nodes (Supplemental Figure 2). The metastatic tumor cells were a major source of the lymphangiogenic factors

Table 1
Characterization of tumors and patients' outcome

pN Stage	Primary tumor stage pT1c diameter	Peritumoral carcinosis primary tumor	Grading	Grading (%)	Intrametastatic carcinosis	Local recurrence	Distant organ metastasis	Death	Follow-up period (months)
Ductal carcinoma									
pN1a a (n = 39)	1.8 ± 0.4 cm	19 (49%)	G1	2 (5%)	0 of 39 (0%)	0	5 (13%)	3 (8%)	54
			G2	22 (56%)					
			G3	15 (39%)					
pN2/3 (n = 20)	1.9 ± 0.3 cm	16 (65%)	G1	3 (15%)	20 of 20 (100%)	2 (10%)	5 (25%)	5 (25%)	56
			G2	8 (40%)					
			G3	9 (45%)					
Lobular carcinoma									
pN1a (n = 17)	1.9 ± 0.35 cm	4 (24%)	G1	0	0 (0%)	0	0	0	55
			G2	14 (82%)					
			G3	3 (18%)					
pN2/3 (n = 12)	1.8 ± 0.6 cm	5 (42%)	G1	0	6 of 12 (50%)	1 (8%)	3 (25%)	3 (25%)	57
			G2	10 (83%)					
			G3	2 (17%)					

Mean age, 58.9 ± 12.8 years. pT1c, primary tumors with diameters between 1–2 cm; pN1a, metastasis in 1–3 axillary lymph node(s), at least 4 larger than 2 mm in greatest diameter; pN2/3, metastases in more than 4 (ipsilateral) lymph nodes, at least 1 larger than 2 mm in greatest diameter. Data applies to all 3 tumor grades.

VEGFC and VEGFA (19), and their expression in the metastasis frequently exceeded that of the corresponding primary tumors (Supplemental Figure 3) and that of mononuclear cells (20) in the adjacent residual lymph node parenchyma or in naive lymph nodes (data not shown). These results suggest that metastatic tumor colonies provide lymphangiogenic factors and coopt the sentinel lymph node's premetastatic lymphatics and extend them by intrametastatic lymphangiogenesis.

We identified carcinoma cell emboli of various sizes within the intrametastatic lymphatic vessels of sentinel lymph nodes (Figure 1). Emboli were present in 100% (20 of 20) of ductal carcinomas with postsentinel lymph node involvement (Table 1), similar to our recent findings in extramammary Paget carcinomas (21). Strikingly, intrametastatic carcinosis was also present in all postsentinel lymph node metastases from individuals with advanced disease (data not shown). In contrast, lymphatic carcinosis was not detected in any of the 56 individuals in whom metastatic tumors were restricted to the sentinel lymph node (Table 1). After mean follow-up of 4.5 years, distant organ metastasis and death were more frequent in the patient group with (25%, 5 of 20 patients) than without intrametastatic lymphatic carcinosis (8%, 3 of 39 patients). The primary tumor's peritumoral lymphatic carcinosis was (statistically nonsignificantly) increased with the incidence of intrametastatic tumor emboli (Table 1). No further correlation of intrametastatic lymphatic carcinosis with luminal, basal, or ERBB2-overexpressing carcinoma subtypes (22) was observed. However, in contrast to ductal carcinomas, we found intrametastatic lymphatic carcinosis only in 50% (6 of 12) of lobular carcinomas with postsentinel lymph node involvement (Table 1). This is in line with previous results showing that the global gene expression of ductal and lobular subtypes differs significantly (23).

Using oligonucleotide arrays, we identified several gene products (DUSP1, RGS1, CYR61, CXCR4, and VEGFC) that were overexpressed in tumor cells of the metastasis compared with primary tumors, and the same discriminatory "markers" were also differentially expressed in intrametastatic lymphatic tumor emboli (Supplemental Figure 4). This indicates that tumor emboli originate from the surrounding metastasis rather than from the primary tumor directly via lymphatics in the premetastatic lymph node.

Bulk invasion of tumor cells into intrametastatic lymphatics. Due to the high density of intrametastatic lymphatics, we frequently observed that tumor cells aggregated into clusters and penetrated in bulk through large discontinuities of the intrametastatic lymphatic's walls (Figure 1). Tumor cell aggregates are located within the vascular lumen, and the vascular walls that border the discontinuity consist of a single endothelial cell layer. This is documented by localization of PROX1 that forms a single "rosary"-like cover around the tumor cells (Figure 1). These histological features are not compatible with surrounding and engulfment of the tumor cell clusters by newly formed lymphatic vessels that would result in a double layer of endothelial cells. Our results favor the interpretation of a direct penetration of the tumor cell aggregates through ruptures in the vascular wall that is also in line with the recent ex vivo observation obtained by video microscopy (24).

An in vitro model of lymphatic invasion. We used an in vitro coculture system to analyze the mechanisms of tumor cell–mediated disruption of lymphatic vessels. This employed spheroids (25, 26) of MCF7 mammary carcinoma cells to reproduce the clusters of cells seen in tumor emboli in vivo. MCF7 cell spheroids remained stable

Table 2
Overexpression of genes in MCF-7 spheroids versus monolayers

Description	Gene	Spheroid/monolayer	*P* value
Gain			
CD44 (Indian blood group)	*CD44*	3.45	0.0039
Intercellular adhesion molecule 1 (CD54)	*ICAM1*	2.67	0.0012
Vascular endothelial growth factor (VEGFA)	*VEGFA*	2.73	0.0100
Selectin L (lymphocyte adhesion molecule 1)	*SELL*	2.45	0.0055
Thrombospondin 2	*THBS2*	2.30	0.0125
Arachidonate 15-lipoxygenase	*ALOX15*	1.89[A]	0.0397
Cadherin 1 type 1, E-cadherin (epithelial)	*CDH1*	1.80	0.0139
Integrin alpha 5 (fibronectin receptor)	*ITGA5*	1.76	0.0370
Loss			
Laminin beta 1	*LAMB1*	–3.87	0.0133
Collagen type XII, alpha 1	*COL12A1*	–4.21	0.0016
Platelet/endothelial cell adhesion molecule (CD31)	*PECAM1*	–1.95	0.0041
Thrombospondin 1	*THBS1*	–1.91	0.0008
Vascular endothelial growth factor C (VEGFC)	*VEGFC*	–1.81	0.0295
Vitronectin	*VTN*	–1.45	0.0559

MCF7 cells were grown as spheroids or as monolayers, and lysed to extract and reverse transcribe RNA for low density arrays (Human Extracellular Matrix and Adhesion Molecules PCR Array; SABiosciences). Genes were identified that are differentially induced or repressed by MCF7 cell spheroid formation and could be related to bulk-like invasion through the lymphatic vasculature. [A]Corresponding gene products were studied in more detail.

for more than 6 hours. When aggregated into spheroids, MCF7 cells changed their gene expression patterns when compared with monolayers and increased their expression of CD44, ICAM1, and VEGFA; they also reduced their expression of matrix components (Table 2). Confluent monolayers of freshly isolated or telomerase "immortalized" (27) human dermal lymphatic endothelial cells were used as surrogates for intrametastatic lymphatics. We found no difference between intra- and extratumoral dermal lymphatics for the expression of several proteins (podoplanin, PROX1, FLT4, biglycan, endoglin, VE-cadherin, variably CD34, and LYVE1) (Supplemental Figure 4), justifying their use for the in vitro studies.

MCF7 spheroids were placed on top of lymphatic endothelial monolayers (Figure 2), which resulted in the highly reproducible formation of circular discontinuities that we designated as circular chemorepellent-induced defects (CCID) in monolayers precisely underneath the MCF7 spheroids. They were highly reminiscent of the defects seen in the lymphovascular walls at sites of tumor cell invasion in vivo. Lymphatic endothelial cells were more than 5 times more sensitive to MCF7 spheroid–induced CCID formation than blood vessel endothelia. CCID formation was not seen using spheroids of the nontumorigenic mammary gland epithelial cell line MCF-10A or human lung fibroblasts (HLFs) (Figure 2).

CCIDs form by migration of lymphatic endothelial cells. Time-lapse videos revealed centrifugal migration of lymphatic endothelial cells strictly beneath the MCF7 spheroids (Figure 2 and Supplemental Video). This correlated also with rearrangement and fragmentation of VE-cadherin in lymphatic endothelial cell junctions at the border of MCF7 spheroid–induced CCIDs (Figure 2). The migratory phenotype of the lymphatic endothelia was confirmed by the localization of the cell movement–associated activated protein phosphatase 1 regulatory inhibitor subunit 12 A (PPP1R12A, MYPT1) (ref. 28 and Figure 2). We discounted a role for apoptosis of lymphatic endothelial cells in the formation of CCIDs by TUNEL and Hoechst 33258 staining both in vitro and in vivo in human sentinel metastases (Supplemental Figure 5).

12(S)-HETE induces CCIDs in lymphatic endothelial cell monolayers. Oligonucleotide array analyses revealed the specific induction of several genes in MCF7 cell spheroids when compared with monolayers, including the hypoxia inducible (29) enzyme 15-lipoxygenase-1 (ALOX15) (Table 2), which metabolizes arachidonic acid to 12[S]-hydroxy-eicosatetraenoic acid (12[S]-HETE) and 15(S)-hydroxyeicosatetraenoic acid (15[S]-HETE). In humans, 12(S)-HETE is produced by ALOX15 and ALOX12, which are the respective products of the *ALOX15* and *ALOX12* genes (30). We have found that MCF7 cells only express *ALOX15* (Table 2), and it was shown previously that they lack *ALOX15B* (31). 12(S)-HETE was identified as a tumor cell–derived retraction factor for blood vessel endothelial cells (32). In lymphatic endothelial monolayers, 12(S)-HETE also transiently reduced VE-cadherin expression (Figure 2). These results fostered the speculation that 12(S)-HETE might be involved in MCF7-induced CCID formation.

We inhibited the enzymatic activity of ALOX15 in MCF7 cells by pharmacologic inhibition with the pan-LOX inhibitor nordihydroguaiaretic acid (33), which resulted in a significant and dose-dependent reduction of MCF7 spheroid–induced CCID areas in lymphatic endothelial cell monolayers (Supplemental Table 2). This result was confirmed with the LOX inhibitor baicalein (34) at nontoxic concentrations (Figure 3 and Supplemental Figure 6), which reduced CCID formation by 90% after 2 hours, and by 40% to 60% after 6 hours of coincubation as determined in pilot experiments (26).

Direct proof for the hypothesis that 12(S)-HETE triggered CCIDs was obtained by placing fibroblast spheroids soaked with synthetic 12(S)-HETE onto lymphatic endothelial cell monolayers. This resulted in CCID formation similar to that induced by MCF7 spheroids, whereas fibroblast spheroids imbibed with 15(S)-HETE or solvent were ineffective (Figure 3). Conversely, blocking 12(S)-HETE with a specific polyclonal antibody (35) inhibited the formation of MCF7 spheroid–induced CCIDs (Figure 3).

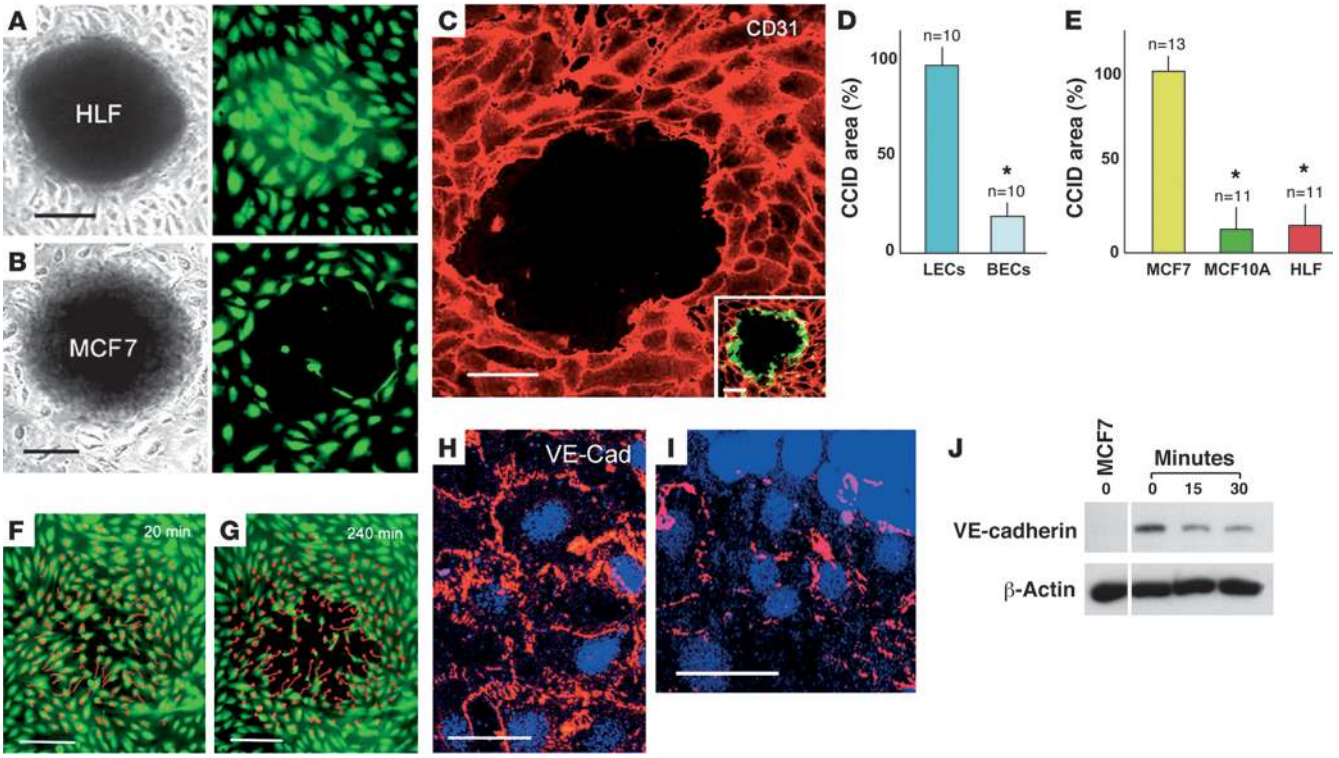

Figure 2

MCF7 cell spheroids induce CCIDs in lymphatic endothelial cell monolayers and disrupt VE-cadherin at the CCIDs. (**A**) Spheroid of HLFs fails to induce any defects in a monolayer of human lymphatic endothelial cells (LECs, Cytotracker tagged in green) after 4 hours of cocultivation. (**B**) MCF7 spheroids induce circular CCIDs. (**C**) A MCF7 spheroid–induced CCID is outlined when the LEC borders are stained for CD31 (red, confocal image). Inset, LECs (demarcated with CD31 in red) at the margin of the CCIDs show expression of PPP1R12A (MYPT1) (green) indicating cell mobility (confocal image). (**D**) MCF7 spheroids induce CCIDs preferentially in LEC monolayers (left bar), but significantly less (14.3% of lymphatics; $*P = 0.0047$) in monolayers of microvascular blood endothelial cells (BECs, right bar). (**E**) When compared with spheroids of MCF7 cells (left bar, 100%), CCID formation in lymphatic monolayers is marginally induced by nonmalignant human breast epithelial cells MCF-10A (9.6% of MCF7 spheroids), and HLFs (11.3%). Data are presented as mean ± SEM. $*P < 0.0001$. (**F** and **G**) Tracings of LEC migration (red lines; starting positions are marked by circles) beneath a spheroid during a 4-hour coincubation. (**H**) Confocal image shows continuous LEC junctions of VE-cadherin (VE Cad) at distance from a spheroid. (**I**) At the spheroid's margin, the VE-cadherin pattern is disrupted. (**J**) Confluent LECs were incubated with 1 μM 12(S)-HETE for 15 and 30 minutes or with solvent (0), and cell lysates were immunoblotted with antibodies to VE-cadherin or β-actin. As controls, VE-cadherin$^-$ MCF7 cells were used. Lanes were run on the same gel but are noncontiguous. Scale bars: 100 μm (**A**, **B**, **F**, and **G**); 25 μm (**C**); 50 μm (**H** and **I**).

These results indicated that CCIDs were induced by MCF7 cell spheroids, which were placed onto the upper side of the lymphatic endothelial monolayer that presumably corresponds to the luminal endothelial aspect in vivo. Here we show that CCIDs were also generated when the MCF7 spheroids were placed onto the basolateral aspects of lymphatic endothelial cells in Transwell chambers (Figure 4).

CCIDs were also obtained with spheroids of tumor lines other than MCF7 cells. This was found for human mammary carcinoma cells (HCC1419, HCC1443, and MDA-MB231) and colon cancer (LS174CoCa, HT29, HTC116), melanoma (CRL1675), and pancreatic adenocarcinoma (PANC1) (Figure 3).

Pharmacological inhibition of cognate mechanisms of tumor invasion and metastasis revealed a minor contribution of metalloproteinases since the pan-matrix-metalloprotease inhibitor GM6001 (36, 37), and specific inhibition of MMP9, TIMP2, and MMP2 reduced CCID formation only by approximately 25%. Reactive oxygen species and cyclooxygenases and their products were not involved (Supplemental Table 2).

Inhibition of 15LOX reduces CCID formation in lymphatic monolayers. Further evidence for the central role of *ALOX15* in CCID formation was obtained by shRNA-mediated knockdown in MCF7 cells (MCF7/*ALOX15*$^-$ cells), which resulted in stable reduction of over 80% of *ALOX15* mRNA as well as 12(S)-HETE and 15(S)-HETE production (Figure 5). Nonmalignant human MCF-10A cells or fibroblasts failed to induce CCIDs, to express *ALOX15* and *ALOX12* genes, and to synthesize 12(S)-HETE (Figure 5). Spheroids of MCF7/*ALOX15*$^-$ cells induced small CCIDs that were similar to baicalein-treated MCF7 spheroids, whereas controls (scrambled shRNA or empty vector–transfected MCF7 cells) were similar to unmodified MCF7 cells. This inhibitory effect of *ALOX15* shRNA was further enhanced by the pan-metalloprotease inhibitor GM6001 (Figure 5). Knocking in of *ALOX12* into MCF7/*ALOX15*$^-$ cells (Supplemental Figure 7) fully reestablished their CCID-forming capacity in the spheroid assay (Figure 5).

Reduced metastatic capacity of ALOX15-deficient tumor cells. We used MCF7 cells with transgene expression of VEGFC (MCF7/*VEGFC* cells) (38, 39) to induce metastasis formation in vivo. Both

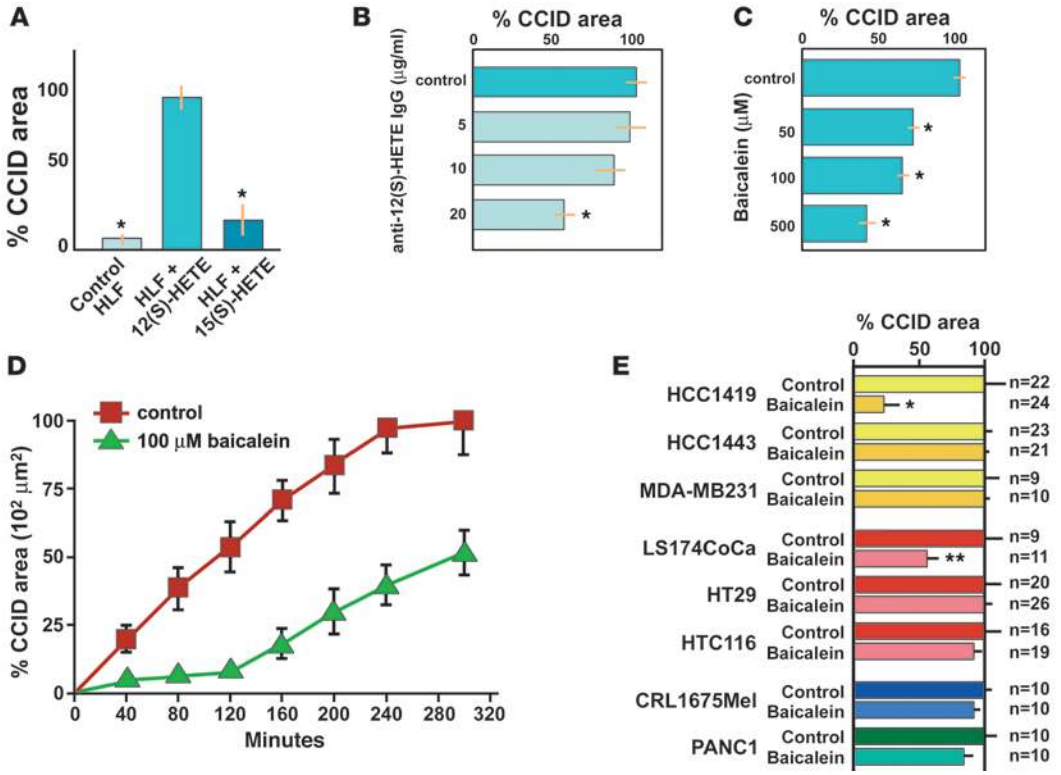

Figure 3

12(S)-HETE causes CCIDs in lymphatic endothelial cell monolayers. (**A**) CCID area in lymphatic endothelial cell monolayers induced by HLF cell spheroids that were presoaked with synthetic 12(S)-HETE ($n = 11$), 15(S)-HETE ($n = 12$), or solvent alone (control; $n = 21$). 12(S)-HETE induced approximately 20 times larger CCIDs than controls (*$P < 0.0001$) after 4 hours of coincubation. (**B**) Antibody against 12(S)-HETE reduces the CCID area by approximately 50% (*$P = 0.0020$). (**C**) The ALOX inhibitor baicalein, a traditional Asian anti-cancer drug, reduces CCID area in a dose-dependent fashion, with the highest dose of 500 μM ($n = 11$) causing reduction to 38% (*$P < 0.0001$) of controls ($n = 20$). (**D**) Time-course incubation over 4 hours with 100 μM baicalein in the media results in approximately 90% reduction of CCID size in the first 2 hours and a gradual increase in CCID formation to more than 50% after 4 hours. (**E**) Spheroids made of the mammary carcinoma cell lines HCC1419, HCC1443, and MDA-MB231 form spheroids that induce CCIDs in lymphatic monolayers, but only HCC1419 cell–mediated CCID formation is sensitive to 100 μM baicalein (inhibition of 78.2%; *$P = 0.0008$). Similarly, spheroids formed from colorectal carcinoma cell lines LS174CoCa, HT29, and HTC116 form CCIDs, but only LS174CoCa are baicalein sensitive (inhibition of 53.3%; **$P = 0.0168$). A melanoma (CRL1675Mel) and a pancreatic carcinoma cell line (PANC1) formed CCIDs in monolayers of lymphatic endothelial cells, but were insensitive (i.e., statistically not significant) to baicalein. All data are presented as mean ± SEM.

VEGFC-overexpressing and unmodified MCF7 cells expressed *ALOX15* and formed CCIDs of similar size in lymphatic monolayers (Supplemental Figure 8). Stable transfection with luciferase (MCF7/*VEGFC/luc*) did not interfere with the expression of other transgenes (data not shown). MCF7/*VEGFC/ALOX15*$^-$*/luc* or control MCF7/*VEGFC/luc* cells that contained scrambled shRNA were injected orthotopically into mammary fat pads of SCID mice. After 32 days, tumors had formed in 100% of animals injected with control MCF7 cells, but only in 50% with MCF7/*VEGFC/ALOX15*$^-$ cells, presumably due to a less receptive micromilieu at the sites of injection, which showed minimal inflammatory infiltration in all cases. However, once established, the xenograft tumors of all MCF7/*VEGFC* cell variants showed similar growth rates, tumor cell turnover, weights, and intratumoral lymphatic vascular densities (Figure 6). At 32 days, 60% of animals in the control groups, but none of the mice bearing MCF7/*ALOX15*$^-$ xenograft tumors, had developed regional lymph node metastases (Figure 6). Sixty-three days after injection, we found lymph node metastases in 100% of control mice, but only in 5% of the MCF7/*ALOX15*$^-$ group. At this end point, the weight of all primary xenograft tumors was similar, and the expression of *VEGFC* transgene and the *ALOX15* shRNA knockdown were unaltered (Figure 6). In xenograft tumors induced by cells of the *ALOX15*-expressing control groups, podoplanin$^+$ and LYVE1$^+$ intratumoral lymphatic vessels had formed that were distended and focally obliterated by tumor emboli at 32 days after injection (38, 39). In contrast, tumors composed of MCF7/*VEGFC/15LOX*$^-$ cells developed collapsed intratumoral lymphatic vessels that were devoid of embolic tumor cells (Figure 6). These in vivo results support the concept that *ALOX15*-driven production of 12(S)-HETE is required for formation of lymph node metastases, by facilitating the entry of tumor cells into intrametastatic lymphatic vessels.

ALOX15 and 12(S)-HETE in human metastases. The relevance of our experimental findings for the formation of human postsentinel lymph node metastases was underscored by immunohistochemical localization of 12(S)-HETE and of ALOX15 in metastatic carcinoma cells in sentinel lymph nodes (Figure 7). This was extended and confirmed by further analysis of tissue arrays containing cores of primary tumors and their corresponding sentinel metastases from

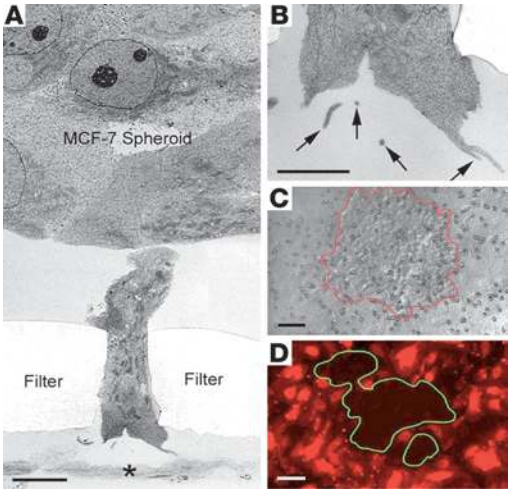

Figure 4
MCF7 tumor cell induced CCID formation in lymphatic monolayers from the abluminal side in Transwell inserts. MCF7 cell spheroids were placed onto the upper side of a filter that was covered by an LEC monolayer on its lower side so that the spheroids were separated from the lymphatic endothelial cells by the filter membrane. Coincubation was performed for 12 hours. (**A**) Low-power electron micrograph of a spheroid extending a "finger" through a filter pore. The LEC monolayer at the basal aspect of the filter shows only extracellular material and debris (*). (**B**) Higher magnification of the tip of the spheroid's extension, showing microvillar or vesicular (arrow) membrane structures, resembling shedding microparticles. (**C**) A spreading spheroid of MCF7 cells (outlined in red) on the upper face of the Transwell membrane. (**D**) At the opposite basal (abluminal) side of the Transwell membrane, a CCID (outlined in green) is formed in the monolayer of lymphatic endothelial cells (tagged red) precisely corresponding to the MCF7 spheroid on the luminal side. Scale bars: 1 μm (**A**); 0.2 μm (**B**); 50 μm (**C** and **D**).

13 patients with ductal carcinomas. These samples were precisely matched for staging pT1c and pN1a. Scoring of immunostaining for ALOX15 (Figure 7) provided evidence for a link between enzyme expression in lymph node metastases and the time of metastasis-free survival, and thus clinical outcome. A similar trend was also observed for the expression of ALOX12 (Supplemental Figure 9).

Discussion

The number of axillary lymph nodes that host metastases of mammary carcinomas is of predictive clinical significance. In this study, we have gained insights into the potential cellular and molecular events involved in metastatic tumor progression from the sentinel to the postsentinel axillary lymph nodes in human mammary carcinomas. This process involves premetastatic conditioning of axillary lymph nodes, invasion of tumor cells into the interconnecting lymphatic vessels, and eventually intranodal tumor cell arrest and proliferation.

Tumors programmed for lymph node metastasis have acquired a specific strategy for premetastatic adaptation of their regional lymph nodes (40, 41), which prominently involves expansion of lymph node sinus and transformation of their lining cells into lymphatic endothelia. This reaction is a stereotypic response to diverse stimuli that range from chemokines and growth factors to lymph congestion by mechanical obliteration of efferent lymphatic vessels (42, 43). However, it is of importance for formation of lymph node metastases and is referred to as *premetastatic lymph node lymphangiogenesis* (41). Moreover, lymphatic vessels develop de novo within the lymph node's metastatic colony and are frequently embolized by tumor cells that phenotypically correspond to cells of the metastasis and not to those in the primary tumors. Intrametastatic lymphangiogenesis occurs in all cases with postsentinel metastasis, and it is also present when the tumor is restricted to the sentinel lymph node. However, only when tumor cells have invaded and embolized the intrametastatic lymphatics do they spread to further lymph nodes downstream, as documented by a 100% correlation of embolization with postsentinel lymph node metastasis, which also applies to further tumor spreading from postsentinel metastases into more distal axillary lymph nodes. This also implies that the intrametastatic lymphatics are connected to the lymph node's efferent lymphatic vessels and is in line with recent experimental evidence (44). Collectively, these results indicate that tumor cell invasion of intrametastatic lymphatic vessels is crucial for lymphatic metastatic tumor dissemination.

These results raise the question of how the tumor cells get access into the intrametastatic lymphatic vasculature. Several pathways of tumor invasion into lymphatic vessels have been observed for different experimental and human tumors (45). One variant implies single tumor cell penetration between or even through endothelial cells, possibly also involving tumor cell epithelial-mesenchymal transition (21, 46, 47). In this investigation, we provide evidence for another pathway for mammary carcinomas similar to that previously described (45), which involves bulk invasion of metastatic tumor cells through large discontinuities of the lymphatic vessel wall. This pathway matches with recent experimental results obtained by in vivo microscopy in which xenografted mammary carcinoma cells spontaneously form mobile cohesive groups that preferentially invade into lymphatic vessels (24).

To gain insights into the mechanisms underlying lymphatic bulk invasion, we have adapted a reductionistic in vitro assay (25, 26) that mimics some features of the in vivo situation. In this system, tumor cell spheroids corresponded to invasive tumor aggregates in vivo, and in lieu of intrametastatic lymphatic vessels, we used monolayers of dermal lymphatic endothelial cells. This choice of endothelial cells was justified because a panel of typical lymphatic genes, including PROX1 and podoplanin, was expressed equally in both normal dermal and intrametastatic lymphatic endothelial cells. In contrast, we have noted that MCF7 cells altered their gene expression program upon spheroid formation and that this includes overexpression of the 12(S)-HETE–producing enzyme ALOX15. The human gene project has revealed 2 *ALOX* isoforms, *ALOX15* and *ALOX15B*. ALOX15B produces 15(S)-HETE only, and there is no evidence that it plays a role in breast cancer pathology (48, 49). In contrast, ALOX15 also generates 12(S)-HETE, which is of relevance for various cancers, including mammary carcinomas (50).

12(S)-HETE was previously shown to increase malignant behavior of some tumors and to reduce it in others (51), and to increase endothelial cell motility and retraction of human umbilical cord endothelial cells (52). This has prompted us to investigate the role of 12(S)-HETE in our in vitro surrogate system of tumor bulk invasion. Our results show that 12(S)-HETE released by MCF7 tumor spheroids induced CCIDs that were formed by centrifugal migration of lymphatic endothelial cells just beneath spheroids. It is possible that this local restriction of endothelial cell mobility could be due to the hydrophobicity

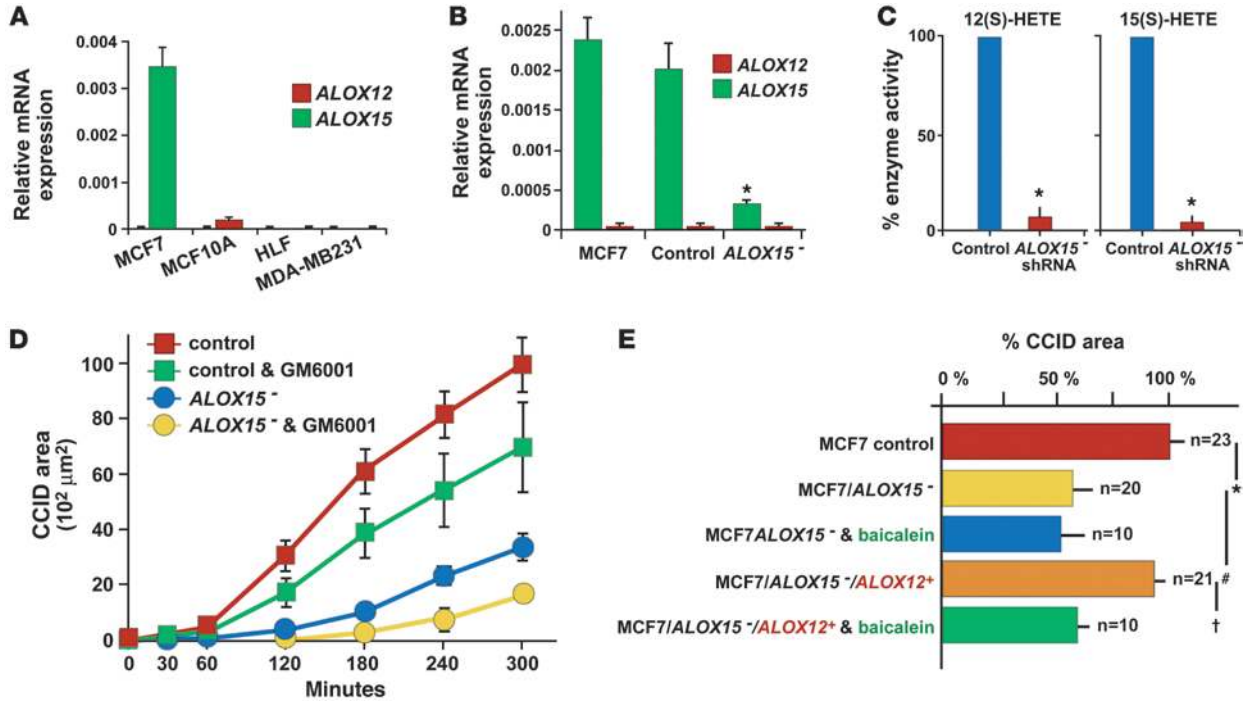

Figure 5

shRNA-mediated knockdown and rescue of lipoxygenase in MCF7 cells. (**A**) The expression of mRNAs of *ALOX15* and *ALOX12* was determined by real-time PCR in MCF7 and MDA-MB231 mammary carcinoma cells and in controls (noncancerous breast epithelial cells MCF-10A and HLFs). MCF7 cells express only *ALOX15* mRNA, but not *ALOX12* mRNA, whereas all other cells fail to produce any of the tested *ALOXs*. (**B**) mRNA levels of *ALOX15* were determined in unmodified MCF7 cells, in control MCF7 cells transduced with scrambled shRNA, and in MCF7/*ALOX15*$^-$ cells. Knockdown of *ALOX15* reduced the expression of *ALOX15* mRNA significantly (*P = 0.0009 compared with vector control) when compared with unmodified or control transduced MCF7 cells. (**C**) Production of 12(S)-HETE and 15(S)-HETE, the arachidonic acid metabolites of ALOX15, is reduced by more than 90% in MCF7/*ALOX15*$^-$ cells when compared with control MCF7 cells that were transduced with scrambled shRNA (*P > 0.0001). (**D**) shRNA-mediated knockdown of *ALOX15* in MCF7 cells (blue line) causes a size reduction similar to that of baicalein in CCID (compare to Figure 3D). This is further aggravated by coincubation with 20 μM of the pan-metalloprotease inhibitor GM6001 (yellow line), which had a similar effect (green line) on controls (MCF7 cells transduced with scrambled shRNA, red line). (**E**) Reconstitution of CCID-forming activity of MCF7/*ALOX15*$^-$ cells by transfection with *ALOX12*. MCF7 spheroid–induced CCID formation is analyzed in the presence or absence of 100 μM baicalein. There is a significant difference in CCID size between MCF7/control versus MCF7/*ALOX15*$^-$ spheroids (*P = 0.0017), MCF7/*ALOX15*$^-$ versus MCF7/*ALOX15*$^-$/*ALOX12*$^+$ spheroids ($^{\#}P$ = 0.0249), and MCF7/*ALOX15*$^-$/*ALOX12*$^+$ spheroids ± baicalein treatment ($^{\dagger}P$ = 0.0331). All data are presented as mean ± SEM.

of 12(S)-HETE that could be released in poorly diffusing membrane microvesicles above its critical micellar concentration (53). However, the actual concentration of 12(S)-HETE in the micromilieu at the spheroid tumor endothelial interface remains to be determined (54). 12(S)-HETE was not toxic for lymphatic endothelial cells, and accordingly, we failed to encounter apoptotic endothelial cells in association with CCIDs. The significance of 12(S)-HETE was confirmed by blocking of CCID formation by a specific antibody or by shRNA-mediated knockdown of the producing enzyme ALOX15. The ability to cause CCIDs was restored by knocking in of *ALOX12*, which also produces 12(S)-HETE and is not expressed in MCF7 cells. 15(S)-HETE, the alternative arachidonic acid metabolite produced by ALOX15, was ineffective. CCID formation was further supported by metalloproteases that loosen the meshwork of VE-cadherin at interendothelial junctions and matrix attachment (36, 37). Taken together, our in vitro findings suggested a hitherto unknown dominant role for ALOX15 and its product 12(S)-HETE in tumor cell–lymphatic endothelial cell interaction. When we extrapolate these in vitro findings to the vascular defects we have observed at sites of tumor cell bulk invasion, it is possible that induction of lymphatic endothelial migration and focal disruption of interendothelial adhesion (e.g., by destabilization of VE-cadherin) could contribute to focal openings in the vascular wall.

Intriguingly, blood endothelial cells were much less sensitive to the migration-inducing effect of 12(S)-HETE than lymphatics. It remains to be determined whether or not this is due to differences in receptor- or nonreceptor-mediated effects. So far, several proteins have been implicated in binding of 12(S)-HETE; however, a definitive universal receptor or receptors are still elusive. We have screened for the expression of 2 putative 12(S)-HETE membrane protein receptors — the leukotriene B_4 receptor (55) and the orphan receptor GPR31 (56) (data not shown) — and failed to detect expression differences between blood and lymphatic endothelial cells. Thus, our results show that 12(S)-HETE preferentially caused CCID formation in lymphatic endothelial monolayers, either by direct interaction with so-far elusive lymphatic receptor or receptors, or indirectly, via currently unidentified intermediaries.

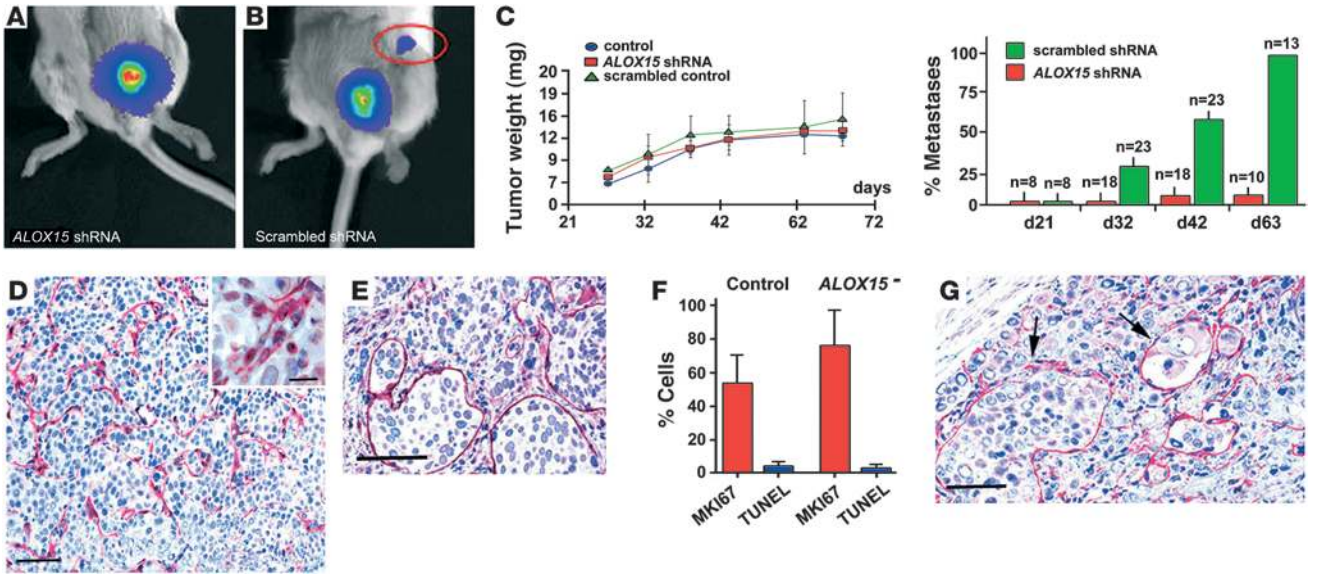

Figure 6

Xenograft tumors induced by *ALOX15* shRNA knockdown cells and control MCF7/*VEGFC* cells expressing luciferase as reporter. (**A**) Bioluminescence image of a xenograft tumor induced by cells that lack *ALOX15* after injection into the fifth mammary fat pad failed to develop lymph node metastases after 32 days. (**B**) Image of a xenograft tumor induced by control MCF7/*VEGFC* cells that were transfected with scrambled shRNA and expressed *ALOX15*, showing a regional lymph node metastasis (red circle). (**C**, left panel) The sizes and growth rates of all xenograft tumors, irrespective of the nature of the inoculated tumor cells (MCF7/*VEGFC*, or MCF7/*VEGFC* cells transfected with scrambled or *ALOX15* shRNA) were similar. (**C**, right panel) Time course of metastasis formation of xenograft tumors induced by MCF7/*VEGFC* cells transfected with *ALOX15* shRNA (red) or with control scrambled shRNA (green) showing that *ALOX15*-deficient MCF7/*VEGFC* were incompetent of metastasis formation. (**D**) Representative picture of a xenograft tumor (same as depicted in **A**). The tumor cells fail to invade into the collapsed intratumoral podoplanin$^+$ lymphatic vessels (red). Insert, tumor embolus–free intratumoral lymphatic vessel with a narrow lumen. (**E** and **G**) Xenograft tumor of the control group (same as in **B**) showing massive tumor intravasation into dilated lymphatic vessels (arrows) that were immunostained for LYVE1 (**E**) or podoplanin (**G**). (**F**) Growth rates of xenograft tumor MCF7/*VEGFC* and MCF7/*VEGFC*/*ALOX15*$^-$ cells were determined by labeling for MKI67 (Ki-67) or by the TUNEL assay. Image analysis revealed a higher (but not significant) MKI67 positivity in *ALOX15*$^-$ tumors compared with control tumors. The rate of apoptosis was similar in both primary tumor types. $n = 6$. Total number of counted nuclei was greater than 2000. Scale bars: 70 μm (**D**, **E**, and **G**); 20 μm (inset). All data are presented as mean ± SEM.

Our results apply primarily to ductal mammary carcinomas that are represented in vitro by MCF7 and HCC1419 cells derived from estrogen receptor–positive ductal carcinomas of the luminal subtype (57). However, only 50% of the lobular mammary carcinomas followed this pattern of tumor spreading. Baicalein-insensitive CCIDs were formed by MDA-MB321 and HCC1443 mammary carcinoma cells that are derived from estrogen receptor–negative ductal carcinomas of the basal subtype and lack ALOXs. This is in contrast to our findings in human tumors and could be due to changes induced by in vitro culturing. Furthermore, the CCID assay suggested that tumors derived from other organs apparently use LOX-independent mechanisms. These include most colorectal carcinomas, melanomas, and a pancreatic cancer. Thus, there is no universal mechanism by which different types of tumors form and propagate lymph node metastases. They apparently also have at their disposal ALOX15-independent mechanisms to enter lymphatic vessels and do not use bulk but rather single-cell invasion, with or without epithelial-mesenchymal transition, possibly depending on TGF-β (24).

These results required verification in a tumor xenograft model that mimics the key findings in sentinel lymph node metastases, i.e., formation of intratumoral lymphatic vessels, bulk invasion of tumor cells, lymphatic embolization, and formation of lymph node metastases. A suitable model for this in vivo proof of principle was found in mouse xenograft tumors produced by human mammary carcinoma MCF7 cells that transgenically overexpress VEGFC (38, 39). This transforms MCF7 cells from nonmetastatic into highly metastatic, with intratumoral lymphangiogenesis, lymph vessel invasion, and embolization, i.e., analogous to human sentinel lymph node metastases. Moreover, we found that MCF7 cells express only a single lipoxygenase, *ALOX15*, and are thus ideally suited for studying the contribution of this enzyme to CCID. shRNA-induced knockdown of *ALOX15* efficiently repressed formation of lymph node metastases. Intratumoral lymphatic vessels were induced both in the control and the *ALOX15* knockdown xenografted tumors. However, in ALOX15-deficient tumors, the lymphatics were collapsed and empty and tumor cells failed to invade and form emboli, in striking contrast to *ALOX15*-expressing and 12(S)-HETE–producing control MCF7 cells. However, we cannot exclude the possibility that the absence of LOX products alters the lymphatic endothelial phenotype to make it less permissive to tumor cell invasion in general.

Here we have brought together 3 correlative observations, i.e., the embolization and invasion of mammary carcinoma cells into intrametastatic lymphatics in human tissues, the 12(S)-HETE–driven formation of CCIDs in vitro, and the important role of the 12(S)-HETE–producing enzyme, ALOX15, for lymph node metastasis formation in mouse xenograft models.

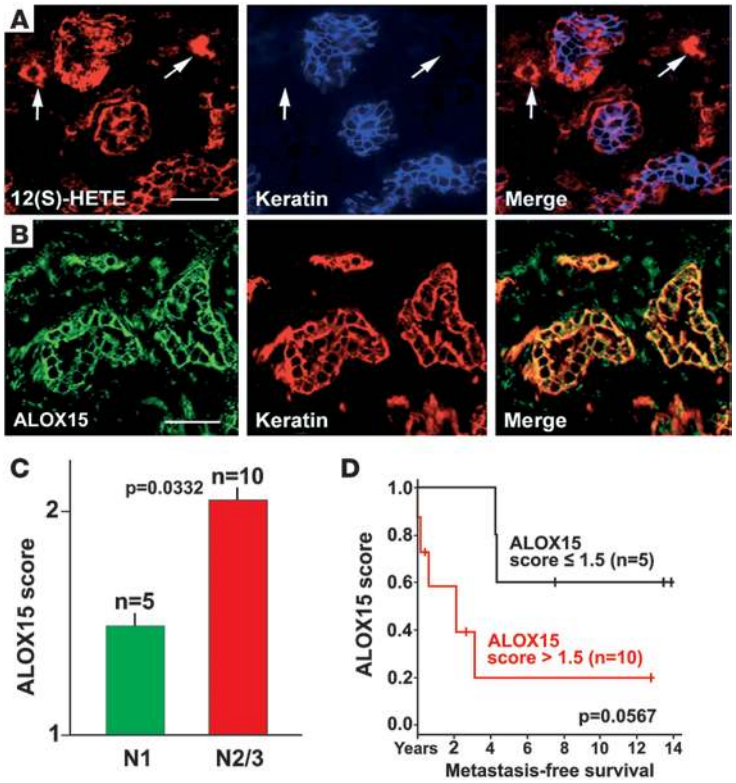

Figure 7
12(S)-HETE and ALOX15 in human sentinel metastases. (**A**) Localization of 12(S)-HETE (red) in the mammary carcinoma cells in a representative sentinel lymph node of a patient with postsentinel lymph node metastasis (total examined: n = 12). 12(S)-HETE colocalizes with tumor cell keratin (blue and merge) and is also expressed by nontumor, presumably inflammatory cells (arrows). (**B**) The 12(S)-HETE–producing enzyme ALOX15 shows a localization similar to that of its product (ALOX15: green; keratin: red). (**C**) Results of the tissue array scoring of the immunostaining for ALOX15 in the tumor cells of the sentinel metastasis in 15 cases of ductal carcinoma. In 5 cases without postsentinel metastases, the score is lower (N1, green column) than in 10 cases with postsentinel spreading (N2/3, red column). (**D**) Metastasis-free survival correlates inversely with the expression of ALOX15 in the tumor cells of the sentinel lymph nodes (P = 0.0507). Scale bars: 50 μm. All data are presented as mean ± SEM.

Taken together, these complementary results favor the hypothesis that 12(S)-HETE–mediated CCID formation is a central event for accession of mammary carcinoma cells into the lymphatic vasculature in sentinels and thus furthers tumor spreading into postsentinel lymph nodes (Supplemental Figure 10).

Do these potential mechanisms of intrametastatic lymphatic invasion also apply to human patients? Our results suggest that this is feasible. Metastatic tumor cells in sentinel lymph nodes of human mammary carcinomas express all the key players, ALOX12, ALOX15, and 12(S)-HETE. In feasibility studies using tissue microarrays of a relatively small number of carefully matched human samples, we found that the abundance of ALOXs is inversely correlated with metastasis-free survival. Pharmacological ALOX inhibition has previously been recognized as antimetastatic and proapoptotic (58, 59) therapy for mammary and other carcinoma cells. Here we show the CCID-reducing efficiency of the ALOX inhibitor baicalein (34), a polyflavone isolated from the roots of *Scuttelaria baicalensis* and still applied in traditional Asian medicine. Thus, our findings could hold the potential that inhibition of ALOX interferes with lymphatic dissemination of ductal mammary carcinomas. Formal clinical studies are required to determine whether or not ALOXs in mammary carcinomas can be used as biomarkers and potential therapeutic targets.

Methods

Selection of cases and tissue samples. Use of human tissue samples and experimental mouse models was approved by the Ethical Committee of the Medical University of Vienna (Approval EK-Nr 270/2006) in compliance with Austrian legislation. We have selected 104 archival cases of mammary carcinomas, classified as NOS, with 69 cases of ductal and 35 of lobular subtype. The patients had not received preoperative neoadjuvant therapy. The primary tumors were matched by their diameters (pT1c, 1–2 ± 0.6 cm), availability of the sentinel, and, when clinically indicated, also postsentinel axillary lymph nodes. Further inclusion criteria were similar sizes of sentinel lymph node metastases (pN1a, >2 mm) and documented follow-up periods of 55 months after surgery. The tumor grading is listed in Table 1. The tumors were also subclassified by immunohistochemistry as luminal, basal, or ERBB2 enriched (22). Sentinel lymph nodes were free of tumors (stage pN0, n = 16) (11), or metastasis was restricted to the sentinel lymph node only (pN1a, n = 56), or also involved additional postsentinel axillary lymph nodes (pN2 or 3, n = 32). All tumors were analyzed for the expression of estrogen and progesterone receptors, the overexpression of ERBB2, and in some cases also for keratins, CD133, CD44, and aldehyde dehydrogenase (60, 61). As controls, naive nontumor-associated lymph nodes were used that were removed during carotid angioplasty or abdominal surgery (n = 16). These nonactivated lymph nodes were devoid of capsular fibrosis, intranodal scars, or activation of germinal centres.

Immunohistochemistry. 4-μm–thick freshly prepared sections from archival paraffin blocks for immunolabeling were processed as described previously (62) using rabbit anti-human podoplanin IgG (5 μg/ml) or with a monoclonal mouse IgG (Bender Med Systems BMS 1105; 1 μg/ml), and anti-human PROX1 rabbit IgG (AngioBio). Some sections were also incubated after podoplanin labeling with monoclonal mouse anti-Ki67 IgG (MIB-1) or anti-human LYVE1 rabbit IgG (DAKO). Rabbit antibodies to 12(S)-HETE (Assay Designs), with less than 2.5% cross-reactivity with 12(R)-HETE and less than 0.3% with 15(S)- and 5(S)-HETE, and ALOX12 and ALOX15 (Abcam) were used on cryostat sections of unfixed primary carcinomas and their sentinel metastases (n = 12). For immunofluorescence, we used appropriate secondary antibodies labeled with Alexa Fluor 488, Alexa Fluor 594, or Alexa Fluor 633 (Molecular Probes). Double-labeling experiments were controlled

by omitting the primary antibodies or by replacement with irrelevant antibodies raised in the same species or of the same mouse IgG subtype. The densities of lymphatic vessels were determined in duplicate by 3 independent observers on unmarked histological sections. We counted the number of lymphatic vessel profiles in at least 30 microscopic fields for each slide, using an objective lens with ×25 magnification. Inter- and intra-observer variations resulted in a "background noise" of 1 vessel per field, and only counts above this threshold were entered into the evaluation. Statistical significance was determined by the *t* test, using the Prism 4 software package (GraphPad). Production and composition of tissue microarrays were performed as described (63). We have carefully selected 15 cases of ductal carcinomas with the identical stages pT1c, pN1a (n = 10), and pT1c, pN2/3 (n = 5).

Isolation and characterization of human dermal lymphatic endothelial cells. Human lymphatic endothelial cells and blood vessel endothelial cells were prepared from commercial (C-12260; PromoCell) or freshly prepared dermal microvascular endothelial cells by sorting with anti-podoplanin and anti-CD31 IgG using Dynabeads (M-280; Dynal 11203) or FACS (FaxStar), as described (64). Also, telomerase "immortalized" lymphatic endothelial cells were used (27). No differences in the expression of other proteins previously thought to distinguish lymphatic vessels outside and within tumors (biglycan, endoglin, CD34, VE-cadherin) were found (Supplemental Figure 4C).

Determination of 12(S)-HETE. 12(S)-HETE and 15(S)-HETE were determined by a reverse-phase high-performance liquid chromatography method (RP-HPLC), as described (65).

Spheroid preparation. Cell spheroids were prepared as described in preliminary experiments (25, 26). Briefly, MCF7 cells were grown in McCoy 5A medium containing 10% fetal calf serum and 1% penicillin/streptomycin (Gibco-BRL; Invitrogen). Noncancerous MCF-10A breast epithelial cells were grown in MEGM medium (CC-3150; Clonetic Bullet Kit) supplemented with bovine pituitary extract, human epithelial growth factor, hydrocortisone, insulin, 1% penicillin/streptomycin, and 10 μM isoproterenol. Normal HLFs were grown in nonessential amino acid media containing 10% fetal calf serum and 1% penicillin/streptomycin and 1% nonessential amino acids.

Low-density real-time PCR arrays. Template cDNAs prepared from total RNA of MCF7 cells grown as monolayer or spheroid were characterized in triplicates using the Human Extracellular Matrix and Adhesion Molecules PCR Array (SABiosciences) and the RT2 SYBR Green/Fluorescein qPCR Master Mix (SABiosciences) on the Chromo4 PCR System (Bio-Rad), following the manufacturer's instructions. The resulting Ct values were analyzed by using the RT2 Profiler PCR Array Data Analysis Template v3.2 (SABiosciences). Genes not included on the low-density real-time array were analyzed by using the following FAM probes obtained from Applied Biosystems: *VEGFA* Hs00173626_m1, *ALOX15* Hs00609608_m1, *ALOX12* Hs00167524_m1, and *ALOX12B* Hs00153961_m1.

MCF-7 spheroid/LEC monolayer cocultivation. In all experiments, telomerase-"immortalized" lymphatic endothelial cells (27) or freshly prepared lymphatic endothelial cells (64) (maximal 6 passages) were used, with identical results. Lymphatic endothelial cells were seeded in EGM2MV medium on 24-well plates and allowed to grow to confluence. Then, the lymphatic endothelial cells (LECs) monolayers were stained with Cytotracker green (2 μg/ml, C2925; Molecular Probes) or Hoechst 33258 (5 μg/ml, H1398; Sigma-Aldrich) at 37°C for 90 minutes. Into each well, 10 MCF7 spheroids were transferred. During the coincubation period, frames were taken at 15-minute intervals with an inverse fluorescence microscope (Zeiss Axiophot) and composed to a time-lapse video. Some preparations were examined in a Zeiss confocal fluorescence microscope.

Transwell culture. Primary or telomerase-immortalized lymphatic endothelial cells were grown on the lower surface of Transwell inserts (membrane diameter 6.5 mm; pore size 8 μm, precoated with 10 μg/ml fibronectin; Costar) until confluent. Then lymphatic endothelial cells were stained with Cytotracker as described above, and tumor cell spheroids were placed onto the upper surface. Coculturing was performed for 24 hours, with fluorescence microscopic control of the LEC monolayer every 180 minutes.

Analysis of CCID formation. Areas of LEC monolayers beneath spheroids were photographed in an Axiovert (Zeiss) fluorescence microscope, using the FITC filter to visualize Cytotracker-stained (green) lymphatic endothelial cells, and the area of CCIDs was measured using Axiovision software (Zeiss).

shRNA knockdown of ALOX15. Lentiviral particles containing shRNA targeting the human *ALOX15* mRNA (SHCLNV-NM_001140) and controls with nonsense shRNA (SHC002V) were obtained from Sigma-Aldrich. MCF7 cells that transgenically overexpress *VEGFC* (38) were seeded onto 24-well plates, and transduced with 2e5 TU in 250 μl MEM containing 10% FCS and 8 μg polybrene/ml by spin infection at 1500 *g* at 32°C for 90 minutes. After incubation for 12 hours, the cells were reseeded onto 100-mm culture plates and selected with 1 μg/ml puromycin for 1 week. Single-cell colonies were tested for knockdown efficiency by real-time PCR, normalizing gene expression to the housekeeping gene *GAPDH*.

Knockin of ALOX12 cDNA. N-terminal *V5*-tag was fused to the *ALOX12* full-length cDNA. The fusion was constructed by PCR (5′ primer: TCAGATCCGCTAGCGGGCGCCATGGGTAAGCCTATCCCTA-ACCCTCTCCTCGGTCTCGATTCTACGGGCCGCTACCGCATCC-GCGTGGCCA, 3′ primer: GGTGGCGGCGGCCGCTCAGATGGT-GACACTGTTCTCTATGCAGCTGGG) using standard PCR conditions and an *ALOX12*-containing expression plasmid (gift from Brigitte Marian, Cancer Research Institute, Vienna, Austria) as template. The primer pair contained 5′ Nhe-I and 3′ Not-I linkers and the PCR product was directly subcloned into pTag-CFP-N (Evrogen) by replacing CFP with the tagged fusion construct. The resulting vector DNA was controlled by sequencing and proper expression of the target gene by Western blotting with a *V5*-tag antibody (Invitrogen) using total lysates of transfected cells.

Xenograft tumors. For xenografting, 10^7 MCF7 cells or their derivatives were dispersed in 30 μl PBS and injected orthotopically into the fat pads of the fifth mammary glands of 8-week-old female SCID mice (Harlan Animal Research Laboratory). 60-day slow-release pellets containing 0.72 mg of 17β-estradiol (Innovative Research of America) were implanted 48 hours previously. Primary tumor growth and formation of metastases were monitored at 10-day intervals by noninvasive bioluminescence imaging using a highly sensitive CCD camera (IVIS 100; Caliper Life Sciences). 150 μg D-luciferin/g of body weight (firefly, potassium salt; Caliper Life Sciences) was injected intraperitoneally. Bioluminescence signals were acquired 18 minutes after application, and normalized signals (photons/sec/cm^2/sr) were evaluated and quantified using Living Image Software (Caliper Life Sciences); the tumor weight was calculated from a calibration curve. The experiment was terminated after 63 days, and primary tumors and lymph node metastases were processed for anti-podoplanin immunohistochemistry or for mRNA determination of *VEGFC*, *ALOX12*, and *ALOX15*, shRNAs, and luciferase. Paraffin sections of formalin-fixed tissues were labeled by the TUNEL assay (Chemicon), MKI67 (KI-67, Novo Castra NCL-Ki67p), and cytokeratin (DAKO Z0622). Fluorescence microscopy was performed on an Axiophot microscope equipped with an AxioCam Colour camera (Zeiss) at a standard magnification of 250. Images were analyzed using ImageJ software package 1.42q (Wayne Rasband, NIH; http://rsb.info.nih.gov/ij).

Statistics. We have used a 2-tailed *t* test for statistical analysis of the experimental data. $P \leq 0.05$ was considered significant. All data are presented as mean ± SEM. The human correlative data were expressed by Kaplan-Meier statistics.

Acknowledgments

This work was supported in part by European Community project LSHG-CT-2004-503573 (Lymphangiogenomics) (to D. Kerjaschki and K. Alitalo); a research fund from the Keyaki-kai Medical Corporation, Tokyo, Japan (to H. Nosaka); by the GenAU project Drug Action by Genomic Networks (DRANGON) (to V. Sexl); by Fonds für Innovative und Interdisziplinäre Krebsforschung der Gemeinde Wien (to G. Krupitza); and by the Austrian Breast and Colorectal Cancer Study Group (ABCSG) (to M. Gnant and M. Rudas). We thank A. Rees for reading the manuscript and A. Jaeger for help with the graphic work.

Received for publication August 13, 2010, and accepted in revised form February 2, 2011.

Address correspondence to: Dontscho Kerjaschki, Clinical Department of Pathology, Allgemeines Krankenhaus Wien, Medical University of Vienna; Waehringer Guertel 18-20, A 1090 Vienna, Austria. Phone: 431.40400.5176; Fax: 431.40400.5193; E-mail: dontscho.kerjaschki@meduniwien.ac.at.

Gregor Bartel's present address is: Department of Internal Medicine III, Medical University of Vienna, Vienna, Austria.

Veronika Sexl's present address is: Department of Pharmacology, Veterinary Medical University, Vienna, Austria.

Hitonari Nosaka's present address is: Department of Internal Medicine, Teikyo University, Tokyo, Japan.

Monika Hämmerle's present address is: Department of Pathology, University of Heidelberg, Heidelberg, Germany.

Helmut Dolznig's present address is: Department of Medical Genetics, Medical University of Vienna, Vienna, Austria.

1. Fidler IJ. The pathogenensis of cancer metastasis: the "seed-and-soil" hypothesis revisited. *Nat Rev Cancer*. 2003;3(6):453–458.
2. Psaila B, Lyden D. The metastatic niche: adapting the foreign soil. *Nat Rev Cancer*. 2009;9(4):285–293.
3. Metha P. Potential role of platelets in the pathogenesis of tumor metastasis. *Blood*. 1984;63(1):55–63.
4. Tammela T, Alitalo K. Lymphangiogenesis: Molecular mechanisms and future promise. *Cell*. 2010; 140(4):460–476.
5. Eyles J, et al. Tumor cells disseminate early, but immunosurveillance limits metastatic outgrowth, in a mouse model of melanoma. *J Clin Invest*. 2010;120(6):2030–2039.
6. Müller-Hermelink N, et al. TNFR1 signaling and IFN-gamma signaling determine whether T-cells induce tumor dormancy or promote multistage carcinogenesis. *Cancer Cell*. 2008;13(6):507–518.
7. Tait CR, Dodwell D, Horgan K. Do metastases metastasize? *J Pathol*. 2004;203(1):515–518.
8. Norton L, Massagué J. Is cancer a disease of self-seeding? *Nat Med*. 2006;12(8):875–878.
9. Ben-Porath I, et al. An embryonic stem cell-like gene expression signature in poorly differentiated aggressive human tumors. *Nat Genet*. 2008; 40(5):499–507.
10. Carlson RW, et al. Breast cancer. Clinical practice guidelines in oncology. *J Natl Compr Canc Netw*. 2009;7(2):122–192.
11. Sobin LH, Gospodarowicz MK, Wittekind C, eds. *TNM Classification of Malignant Tumours (Uicc International Union Against Cancer)*. New York, New York, USA: Wiley-Blackwell; 2009.
12. Britton TB, Solanki CK, Pinder SE, Mortimer PS, Peters AM, Purushotham AD. Lymphatic drainage pathways of the breast and the upper limb. *Nucl Med Commun*. 2009;30(6):427–430.
13. Van den Eynden G, et al. Increased sentinel lymphnode lymphangiogenesis is associated with non-sentinel axillary lymph node involvement in breast cancer patients with a positive sentinel node. *Clin Cancer Res*. 2007;13(18 pt 1):5391–5397.
14. Breiteneder-Geleff S, et al. Angiosarcomas express mixed endothelial phenotypes of blood and lymphatic capillaries: podoplanin as a specific marker for lymphatic endothelium. *Am J Pathol*. 1999;154(2):385–394.
15. Banerji S, et al. LYVE1, a new homologue of the CD44 glycoprotein, is a lymph-specific receptor for hyaluronan. *J Cell Biol*. 1999;144(4):789–801.
16. Wigle JT, Oliver G. Prox1 function is required for the deveLOXpment of the murine lymphatic system. *Cell*. 1999;98(6):769–778.
17. Marinho VF, Metze K, Sanches FS, Rocha GF, Gobbi H. Lymph vascular invasion in invasive mammary carcinomas identified by the endothelial lymphatic marker D2-40 is associated with other indicators of poor prognosis. *BMC Cancer*. 2008;8:64.
18. Van den Eynden GG, et al. Induction of lymphangiogenesis in and around axillary lymph node metastases of patients with breast cancer. *Br J Cancer*. 2006;95(10):1362–1366.
19. Hirakawa S, Kodama S, Kunstfeld R, Kajiya K, Brown LF, Detmar M. VEGFA induces tumor and sentinel lymph node lymphangiogenesis and promotes lymphatic metastasis. *J Exp Med*. 2005;201(7):1089–1099.
20. Schoppmann SF, et al. Tumor-associated macrophages express lymphatic endothelial growth factors and are related to peritumoral lymphangiogenesis. *Am J Pathol*. 2002;161(3):947–956.
21. Hirakawa S, et al. Nodal lymphangiogenesis and metastasis: Role of tumor-induced lymphatic vessel activation in extramammary Paget's disease. *Am J Pathol*. 2009;175(5):2235–2248.
22. Sotiriou C, et al. Breast cancer classification and prognosis based on gene expression profiles from a population-based study. *Proc Natl Acad Sci U S A*. 2003;100(18):10393–10398.
23. Bertucci F, et al. Lobular and ductal carcinomas of the breast have distinct genomic and expression profiles. *Oncogene*. 2008;27(40):5359–5372.
24. Giampieri S, Manning C, Hooper S, Jones L, Hill CS, Sahai E. Localized and reversible TGFbeta signalling switches breast cancer cells from cohesive to single cell motility. *Nat Cell Biol*. 2009; 11(11):1287–1296.
25. Offner FA, et al. Interaction of human malignant melanoma tumor spheroids with endothelium and reconstituted basement membrane: modulation by RGDS. *Int J Cancer*. 1993;54(3):506–512.
26. Madlener S, et al. Multifactorial anticancer effects of digalloyl-resveratrol encompass apoptosis, cell cycle arrest, and inhibition of lymphendothelial gap formation in vitro. *Br J Cancer*. 2010;102(9):1361–1370.
27. Schoppmann SF, et al. Telomerase-immortalized lymphatic and blood vessel endothelial cells are functionally stable and retain their lineage specificity. *Microcirculation*. 2004;11(3):261–269.
28. Matsumura F, Hartshorne DJ. Myosin phosphatase target subunit: Many roles in cell function. *Biochem Biophys Res Commun*. 2008;369(1):149–156.
29. Hultén LM, et al. 15-Lipoxygenase-2 is expressed in macrophages in human carotid plaques and regulated by hypoxia-inducible factor-1alpha. *Eur J Clin Invest*. 2010;40(1):11–17.
30. Funk CD. The molecular biology of mammalian lipoxygenases and the quest for eicosanoid functions using lipoxygenase-deficient mice. *Biochim Biophys Acta*. 1996;1304(1):65–84.
31. Subbarayan V, et al. Inverse relationship between 15-lipoxygenase-2 and PPAR-gamma gene expression in normal epithelia compared with tumor epithelia. *Neoplasia*. 2005;7(3):280–293.
32. Honn KV, et al. Tumor cell-derived 12(S)-hydroxyeicosatetraenoic acid induces microvascular endothelial cell retraction. *Cancer Res*. 1994; 54(2):565–574.
33. Funk CD. Lipoxygenase pathways as mediators of early inflammatory events in atherosclerosis. *Arterioscler Thromb Vasc Biol*. 2006;26(6):1204–1206.
34. Li-Weber M. New therapeutic aspects of flavones: the anticancer properties of Scutellaria and its main active constituents Wogonin, Baicalein and Baicalin. *Cancer Treat Rev*. 2009;35(1):57–68.
35. González-Núñez D, Claria J, Rivera F, Poch E. Increased levels of 12(S)-HETE in patients with essential hypertension. *Hypertension*. 2001;37(2):334–338.
36. Deryugina EI, Quigley JP. Matrix metalloproteinases and tumor metastasis. *Cancer Metastasis Rev*. 2006;25(1):9–34.
37. Baker AH, Edwards DR, Murphy G. Metalloproteinase inhibitors: biological actions and therapeutic opportunities. *J Cell Sci*. 2002;115(pt 19):3719–3727.
38. Karpanen T, et al. Vascular endothelial growth factor C promotes tumor lymphangiogenesis and intralymphatic tumor growth. *Cancer Res*. 2001;61(5):1786–1790.
39. He Y, et al. Vascular endothelial cell growth factor receptor 3-mediated activation of lymphatic endothelium is crucial for tumor cell entry and spread via lymphatic vessels. *Cancer Res*. 2005;65(11):4739–4746.
40. Ran S, Volk L, Hall K, Flister MJ. Lymphangiogenesis and lymphatic metastasis in breast cancer. *Pathophysiology*. 2010;17(4):229–251.
41. Mumprecht V, Detmar M. Lymphangiogenesis and cancer metastasis. *J Cell Mol Med*. 2009; 13(8A):1405–1416.
42. Steinmann G, Földi E, Földi M, Rácz P, Lennert K. Morphologic findings in lymph nodes after occlusion of their efferent lymphatic vessels and veins. *Lab Invest*. 2009;47(1):43–50.
43. Angeli V, et al. B cell-driven lymphangiogenesis

in inflamed lymph nodes enhances dendritic cell mobilization. *Immunity*. 2006;24(2):203–215.
44. Harrell MI, Iritani BM, Ruddell A. Tumor-induced sentinel lymph node lymphangiogenesis and increased lymph flow precede melanoma metastasis. *Am J Pathol*. 2007;170(2):774–786.
45. Carr I. Lymphatic metastasis. *Cancer Metastasis Rev*. 1983;2(3):307–317.
46. Azzali G. Tumor cell transendothelial passage in the absorbing lymphatic vessel of transgenic adenocarcinoma mouse prostate. *Am J Pathol*. 2007;170(1):334–346.
47. Yang J, et al. Twist, a master regulator of morphogenesis, plays an essential role in tumor metastasis. *Cell*. 2004;117(7):927–939.
48. Tang DG, Bhatia B, Tang S, Schneider-Broussard R. 15-lipoxygenase 2 (15-LOX2) is a functional tumor suppressor that regulates human prostate epithelial cell differentiation, senescence and growth (size). *Prostaglandins Other Lipid Mediat*. 2007;82(1–4):135–146.
49. Brash AR, Boeglin WE, Chang MS. Discovery of a second 15S-lipoxygenase on humans. *Proc Natl Acad Sci U S A*. 1997;94(12):6148–6152.
50. Jiang WG, Douglas-Jones A, Mansell RE. Levels of expression of lipoxygenases and cycloxygenase 2 in human breast cancer. *Prostaglandins Leukot Essent Fatty Acids*. 2003;69(4):275–281.
51. Bhattacharya S, Mathew G, Jayne DG, Pelengaris S, Khan M. 15-lipoxygenase-1 in colorectal cancer: a review. *Tumour Biol*. 2009;30(4):185–199.
52. Honn KV, et al. Enhanced endothelial cell retraction mediated by 12(S)-HETE: a proposed mechanism for the role of platelets in tumor cell metastasis. *Exp Cell Res*. 1994;210(1):1–9.
53. Uchide K, Sakon M, Ariyoshi H, Nakamori S, Tokunaga M, Monden M. Cancer cells cause vascular endothelial cell (vEC) retraction via 12(S)HETE secretion; the possible role of cancer cell derived microparticle. *Ann Surg Oncol*. 2007;14(2):862–868.
54. Moreno JJ. New aspects of the role of hydroxyeicosatetraenoic acids in cell growth and cancer development. *Biochem Pharmacol*. 2009;77(1):1–10.
55. Kim GY, Lee JW, Cho SH, Seo JM, Kim JH. Role of the low-affinity leukotriene B4 receptor BLT2 in VEGF-induced angiogenesis. *Arterioscler Thromb Vasc Biol*. 2009;29(6):915–920.
56. Guo Y, Nie D, Honn KV. Cloning and identification of a G-protein coupled receptor for 12(S)-HETE. *Proc Amer Assoc Cancer Res*. 2004;45:2746.
57. Neve RM, et al. A collection of breast cancer cell lines for the study of functionally distinct cancer subtypes. *Cancer Cell*. 2006;10(6):515–527.
58. Umezawa K. Inhibition of experimental metastasis by enzyme inhibitors from microorganisms and plants. *Adv Enzyme Regul*. 1996;36:267–81.
59. Tong WG, Ding XZ, Adrian TE. The mechanisms of lipoxygenase inhibitor-induced apoptosis in human breast cancer cells. *Biochem Biophys Res Commun*. 2002;296(4):942–948.
60. Russo J, et al. The concept of stem cell in the mammary gland and its implication in morphogenesis, cancer and prevention. *Front Biosci*. 2006; 11:151–172.
61. Charafe-Jauffret E, Monville F, Ginestier C, Dontu G, Birnbaum D, Wicha MS. Cancer stem cells in breast: current opinion and future challenges. *Pathobiology*. 2008;75(2):75–84.
62. Wick N, et al. Lymphatic precollectors contain a novel, specialized subpopulation of podoplanin low, CCL27-expressing lymphatic endothelial cells. *Am J Pathol*. 2008;173(4):1202–1209.
63. Vinatzer U, et al. Expression of HER2 and the coamplified genes GRB7 and MLN64 in human breast cancer: quantitative real-time reverse transcription-PCR as a diagnostic alternative to immunohistochemistry and fluorescence in situ hybridization. *Clin Cancer Res*. 2005;11(23):8348–8357.
64. Kriehuber E, et al. Isolation and characterization of dermal lymphatic and blood endothelial cells reveal stable and functionally specialized cell lineages. *J Exp Med*. 2001;194(6):797–808.
65. Werz O, Steinhilber D. Selenium-dependent peroxidases suppress 5-lipoxygenase activity in B-lymphocytes and immature myeloid cells. The presence of peroxidase-insensitive 5-lipoxygenase activity in differentiated myeloid cells. *Eur J Biochem*. 1996;242(1):90–97.